

Elliptic instability in a Rankine vortex with axial flow

Laurent Lacaze,^{a)} Anne-Laure Birbaud, and Stéphane Le Dizès

Institut de Recherche sur les Phénomènes Hors Equilibre, 49 rue F. Joliot-Curie, F-13384 Marseille Cedex 13, France

(Received 30 January 2004; accepted 21 September 2004; published online 23 November 2004)

The elliptic instability of a Rankine vortex with axial flow subject to a weak strain field perpendicular to its axis is analyzed by asymptotic methods in the limit of small strain rate. General unstable modes associated with resonant Kelvin modes of arbitrary azimuthal wavenumbers are considered. Both the effects of axial flow and viscosity are analyzed in details. © 2005 American Institute of Physics. [DOI: 10.1063/1.1814987]

I. INTRODUCTION

A stable vortex can become unstable when it is placed in a strain field that deforms its streamlines into ellipses. This so-called elliptic instability is due to the resonance of two Kelvin modes with the external strain field associated with the elliptic deformation. The aim of this paper is to study the effect of an axial flow on the characteristics of this instability.

The elliptic instability in a vortex without axial flow has already been the interest of many works. It has also been observed in various geometries, which could be relevant either to geophysical applications, or industrial issues. The reader is referred to the review of Kerswell¹ for a list of references. The elliptic instability is also present in open flows. In particular, it plays an important role in the dynamics of vortices generated by aircraft. In the aeronautical context, the elliptic deformation of the vortex is due to the strain field induced by the other vortices present in the wake. So far, the elliptic instability has permitted to explain the three-dimensional transition in both counterrotating vortex pairs² and corotating vortex pairs.³ Several analytical models have been constructed^{4–6} but none of them contains the axial flow that should be present in airplane trailing vortices.^{7,8}

In the present work, we analyze the effect of such an axial flow. We consider an idealized vortex model (the Rankine vortex) in order to analyze this effect by semianalytical methods. The stability properties of the Rankine vortex with axial flow have been calculated by Lessen *et al.*⁹ and Loiseleux *et al.*¹⁰ Without external strain field, they have shown that this vortex possesses an unstable mode and infinitely many neutral Kelvin modes. Here, our goal is to consider these neutral modes and to analyze the conditions under which they can be resonantly excited by a strain field. Our approach follows the asymptotic analysis developed in Refs. 11–14. The small parameter of the analysis is the ratio of the external strain rate by the vorticity.

Moore and Saffman¹² also considered the effect of a weak axial flow on the elliptic instability characteristics. But their analysis was limited to axial flow parameter of the order of our small parameter. They showed, in a general set-

ting, that weak axial flow tends to create a stabilizing frequency detuning if the axial wavenumber is fixed. Contrarily to Moore and Saffman analysis, in the present study, the axial flow is not small. Moreover, the characteristics of the resonant modes are allowed to vary with the axial flow parameter such that the detuning effect discovered by Moore and Saffman¹² is not present.

II. SMALL STRAIN ANALYSIS

We consider a basic flow whose velocity field in cylindrical coordinates (r, θ, z) is of the form

$$\mathbf{U} = (0, r, W_0) + \varepsilon[-r \sin(2\theta), -r \cos(2\theta), 0], \quad r \leq 1,$$

$$\mathbf{U} = \left(0, \frac{1}{r}, 0\right) + \varepsilon \left[-\frac{1}{2} \left(r + \frac{1}{r^3} \right) \sin(2\theta), -\frac{1}{2} \left(r - \frac{1}{r^3} \right) \cos(2\theta), 0 \right], \quad r > 1, \quad (1)$$

up to $O(\varepsilon)$ terms, where ε is the small strain rate. The leading order terms correspond to the Rankine vortex with con-

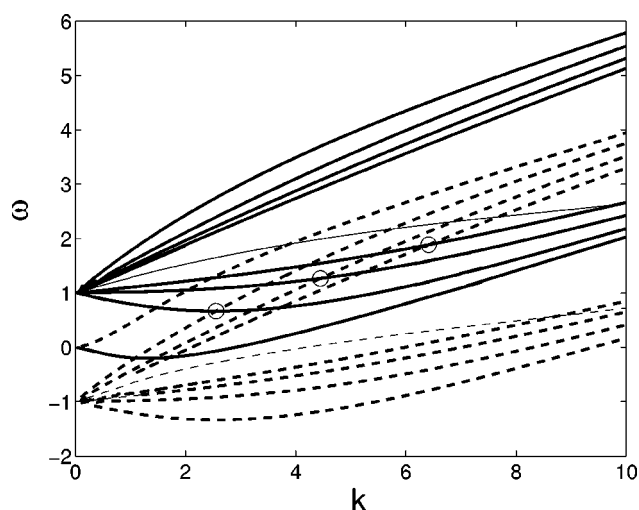


FIG. 1. Eigenfrequencies vs k for $m=-1$ (dashed line) and $m=1$ (line) for an axial parameter $W_0=0.3$. The thin lines represent the real part of the frequency of the Kelvin–Helmholtz mode. The Kelvin–Helmholtz mode is here always unstable.

^{a)}Author to whom correspondence should be addressed. Electronic mail: lacaze@irphe.univ-mrs.fr

TABLE I. Critical axial flow parameter W_0 and critical axial wavenumber k_s for various m associated with the Kelvin–Helmholtz instability. The Kelvin–Helmholtz mode is unstable for $W_0 < W_{0_s}$ or $k > k_s$, but it can be neutral if none of these conditions is satisfied.

m	-7	-6	-5	-4	-3	-2	-1	1	2	3	4	5	6	7
W_{0_s}	0.48	0.55	0.64	0.76	0.96	1.32	2.17	2.08	1.41	1.11	0.94	0.81	0.73	0.65
k_s	0.92	0.80	0.69	0.58	0.47	0.34	0.22	0.29	0.51	0.69	0.85	0.99	1.12	1.24

stant axial flow. Here, the vortex radius and the angular velocity in the core have been chosen to nondimensionalize all the quantities. The parameter W_0 measures the strength of the axial flow. It is the inverse of the so-called Swirl number. The order ε terms in (1) represent the small strain field which elliptically deforms the vortex. As shown by Tsai and Widnall¹¹ and Moore and Saffman,¹² it is these terms which are the source of instability. The mechanism is the following. Two Kelvin modes associated with the leading order flow can resonate with the weak strain field. This resonance occurs if two normal modes defined by their frequency ω , axial wavenumber k , and azimuthal wavenumber m satisfy the following conditions:

$$\omega_2 = \omega_1, \quad k_2 = k_1, \quad m_2 - m_1 = \pm 2. \quad (2)$$

It leads to an inviscid temporal growth of the two coupling mode amplitudes with a characteristic growth rate proportional to ε . Normal modes for the Rankine vortex with axial flow can be calculated explicitly.¹⁰ As for the Rankine vortex without axial flow, there exist an infinity of nonviscous neutral modes which are associated with the fluid rotation.¹⁵ Their frequencies are such that

$$-2 < \omega - m - kW_0 < 2.$$

There exists an additional mode which is due to the axial velocity jump across the vortex core boundary (see Fig. 1). This mode is associated with the Kelvin–Helmholtz instability: its growth rate for large axial wavenumber k is $\sigma \sim W_0 k$. This Kelvin–Helmholtz mode is, however, strongly affected by the Kelvin neutral modes for small k . As shown by Loiseleux *et al.*,¹⁰ it can even become neutral, in small wavenumber intervals satisfying $k < k_s(m)$ if W_0 is above a critical value $W_{0_s}(m)$. Loiseleux *et al.*¹⁰ provided $k_s(-1)$ and $W_{0_s}(-1)$. Values of $k_s(m)$ and $W_{0_s}(m)$ are given in Table I for other m . For a given m , if $k < k_s(m)$ and $W > W_{0_s}(m)$, the neutrally stable Kelvin–Helmholtz mode becomes a new candidate for resonance. Yet, we have found that it never satisfies the resonance condition (2) with any other modes whatever m . Thus, it could not intervene in the elliptic instability.

When the Kelvin–Helmholtz mode is unstable (in particular, if $k > k_s$ or $W < W_{0_s}$), it cannot be considered as a possible mode in the resonance condition because this condition only applies to neutral modes. For this reason, it has to be dismissed from the analysis. Moreover, it is worth mentioning that this unstable mode, which is obtained here for small axial flow, is not expected to be always present in other vortices. For more realistic vortices such as the Batchelor vortex (Gaussian profiles), nonviscous instability only occurs

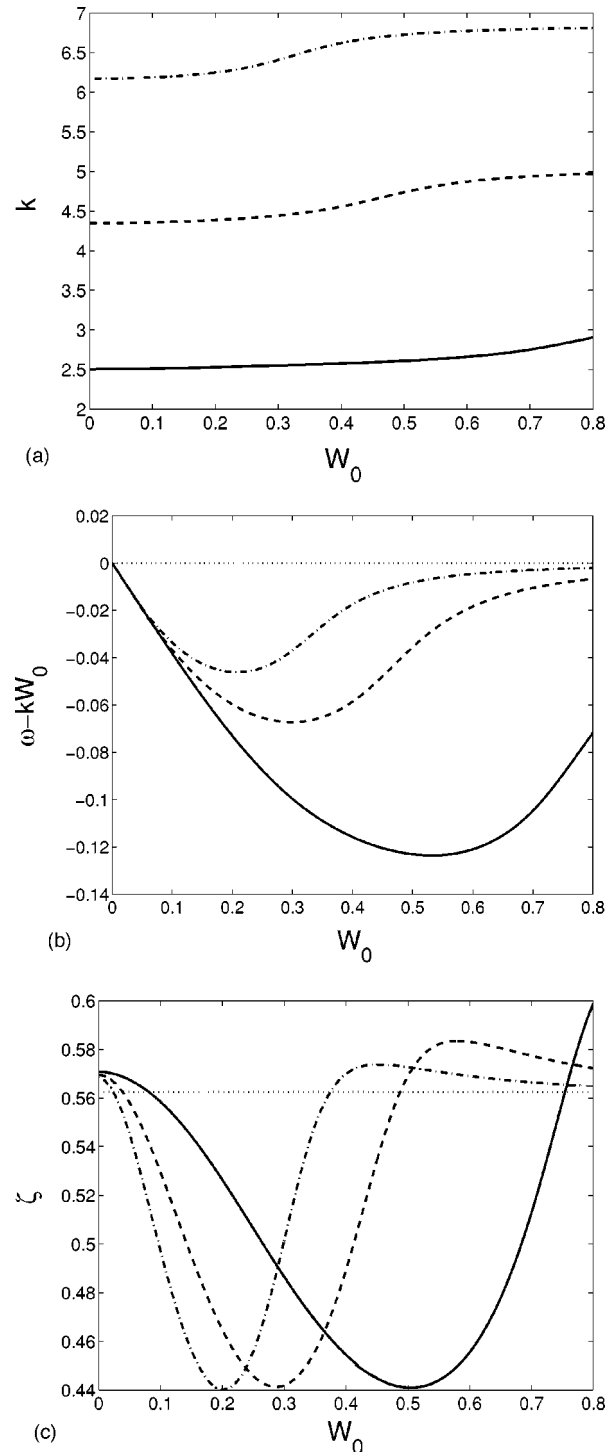


FIG. 2. Characteristics of the first three principal modes for $(m_1, m_2) = (-1, 1)$. Solid, dashed, and dash-dot lines are, respectively, the first, second, and third principal modes. (a) Axial wavenumber k . (b) Convective frequency $\omega - kW_0$. (c) Coupling coefficient ζ (also equal to the nonviscous growth rate normalized by the strain rate).

TABLE II. Characteristics of the principal modes close to ideal resonance.

Modes	(m_1, m_2)	$(-4, -2)$			$(-3, -1)$			$(-2, 0)$			$(-1, 1)$		
	i	1	2	3	1	2	3	1	2	3	1	2	3
W_0		0.1309	0.0527	0.0268	0.1698	0.0529	0.0240	0.2563	0.0456	0.0176	0	0	0
$\omega - kW_0$		-3.0023	-3.0025	-3.0013	-2.0091	-2.0031	-2.0014	-1.0329	-1.0035	-1.0015	0	0	0
k		3.0521	5.0044	6.8832	2.3259	4.2191	6.0734	1.5505	3.3842	5.2321	2.505	4.349	6.174
ζ		0.5850	0.5707	0.5679	0.5876	0.5710	0.5683	0.5901	0.5710	0.5686	0.5708	0.5695	0.5681

when the axial flow is sufficiently large ($W_0 \geq 0.6$).¹⁶ This means that for the Batchelor vortex there is no unstable Kelvin–Helmholtz modes for small axial flow. This provides a physical justification for dismissing the unstable Kelvin–Helmholtz mode from the analysis.

As shown by Eloy and Le Dizès¹³ for the Rankine vortex without axial flow, a combination of two neutral modes satisfying the condition of resonance is always destabilized by the strain field. The growth rate can be calculated by a perturbation method. The method is classical and the analysis of Eloy and Le Dizès¹³ can be applied to the present case almost without any modification. The final result is an expression for the growth rate σ which reads

$$\frac{\sigma}{\varepsilon} = \sqrt{\zeta^2 + \frac{1}{4}(\nu_{m_1} - \nu_{m_2})^2} - \frac{1}{2}(\nu_{m_1} + \nu_{m_2}). \tag{3}$$

In this expression, ζ is the destabilizing term which is associated with the coupling of the resonant mode with the strain field. It provides the inviscid growth rate as $\sigma_{nv} = \zeta\varepsilon$. The coefficients ν_{m_1} and ν_{m_2} are viscous damping terms of order $1/(\varepsilon \text{Re})$. In order to keep these terms in (3), it is implicitly assumed that $\text{Re} = O(1/\varepsilon)$. As demonstrated by Eloy and Le Dizès,¹³ it is important to consider viscous effects on the perturbation to understand the mode selection in

more realistic configurations. Viscous damping will always tend to stabilize resonant configurations of large wavenumber. It also favors the unstable modes with the smallest wavenumbers which is in agreement with all the experimental observations of the elliptic instability.

In Fig. 1 are displayed the normal mode frequencies ω versus k for two azimuthal wavenumbers $m=1$ and $m=-1$ and for a fixed axial parameter $W_0=0.3$. Each branch crossing, except those involving the Kelvin–Helmholtz branch indicated by thin lines, corresponds to a resonant configuration. Yet, these unstable configurations do not exhibit the same growth rate. As demonstrated by Eloy and Le Dizès¹³ for the Rankine vortex without axial flow, resonant configurations associated with the crossing of two branches of same label, possess a growth rate much larger than the others. This feature is also observed in presence of axial flow. As in Eloy and Le Dizès,¹³ these resonant configurations will be called “principal modes.” The first three principal modes for the azimuthal wavenumbers $m=1$ and $m=-1$, noted $(-1, 1, i)$ $i = 1, 2, 3$, are indicated by small circles in Fig. 1. In the following section, the condition of resonance (2) is analyzed for various couples of azimuthal wavenumbers (m_1, m_2) as a function of W_0 . The characteristics of the first principal modes and the coefficients ζ , ν_{m_1} , and ν_{m_2} in their growth rate expression (3) are computed.

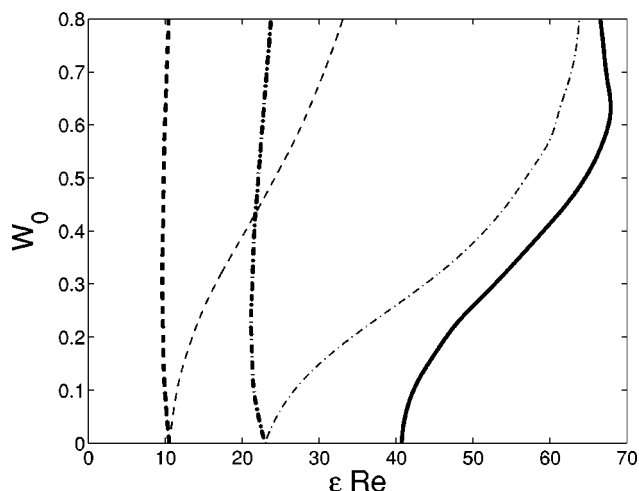


FIG. 3. Marginal stability curve for the resonant modes of azimuthal wavenumbers m_1 and m_2 . Solid line, $(m_1, m_2) = (-1, 1)$; bold dashed line, $(m_1, m_2) = (0, 2)$; thin dashed line, $(m_1, m_2) = (0, -2)$; bold dash-dot line, $(m_1, m_2) = (1, 3)$; thin dash-dot line, $(m_1, m_2) = (-1, -3)$.

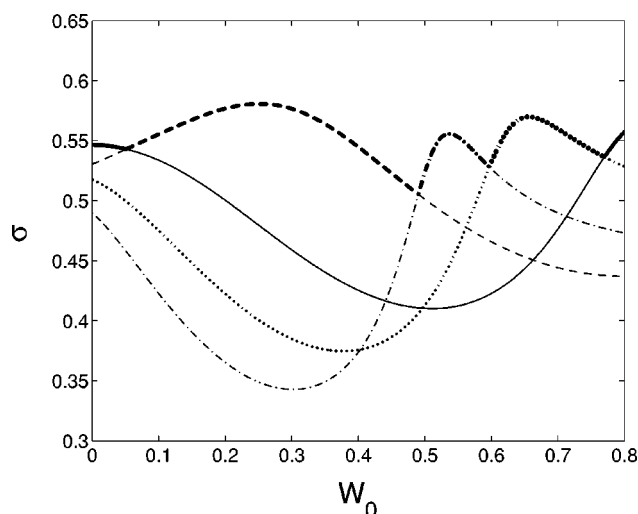


FIG. 4. Viscous growth rate of four more unstable modes as W_0 varies for $\varepsilon \text{Re} = 950$. Solid line, $(-1, 1, 1)$; dashed line, $(-2, 0, 1)$; dash-dot line, $(1, 3, 2)$; dotted line, $(0, 2, 2)$.

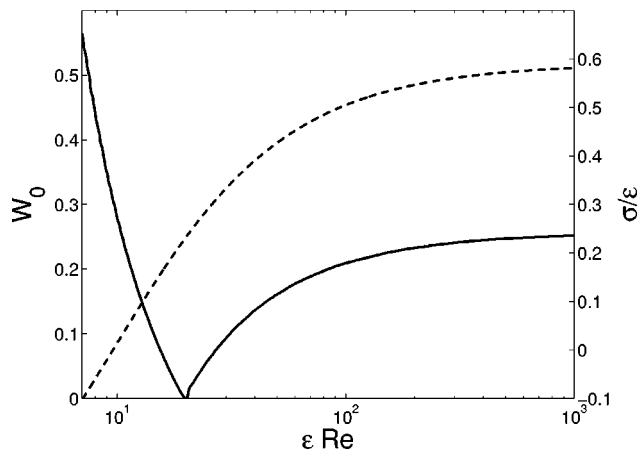


FIG. 5. Most dangerous axial flow parameter W_0 (solid line) and corresponding maximum growth rate (dashed line) as a function of εRe .

III. RESULTS

In Figs. 2(a) and 2(b) are plotted as a function of W_0 the characteristics of the first three resonant modes for $(m_1, m_2) = (-1, 1)$. The coupling coefficient ζ is shown in Fig. 2(c). It measures the nonviscous growth rate normalized by the strain rate. The dotted line in Fig. 2(c) is the local estimate $\zeta = 9/16$ obtained by Waleffe¹⁷ by considering the vortex core only. As shown by Eloy and Le Dizès¹³ for a Rankine vortex without axial flow, this estimate is also obtained for the growth rate of principal modes if their frequency is close to $(m_1 + m_2)/2$. Similar results are observed in the presence of axial flow. The local estimate of Waleffe¹⁷ is not modified by axial flow. However, one can easily show that the principal mode frequency must satisfy

$$\omega = \frac{m_1 + m_2}{2} + kW_0 \quad (4)$$

in addition to (2), to reach the local estimate. In the sequel, we shall denote this condition as the condition of “ideal resonance.” The condition of ideal resonance is shown by a dotted line in Fig. 2(b). Upon comparing the plots in Figs. 2(b) and 2(c), one can see that there is a good correlation between the growth rate curve and the gap between mode frequency and ideal frequency. When the gap is the largest, the growth rate is the smallest. This correlation becomes even better as k increases for a fixed W_0 . These features were also observed in the Rankine vortex without axial flow.¹³ Note, however, that without axial flow, the principal modes $(-1, 1)$ were all “ideally” resonant because of the symmetry of the dispersion relation $\omega(-m) = -\omega(m)$. When an axial flow is present, as this symmetry is broken, no principal mode is *a priori* ideally resonant. It is only for particular values of W_0 that the frequency of a given principal mode can satisfy (4). Such values of W_0 are given in Table II for a few principal modes of negative azimuthal wavenumbers. For positive azimuthal wavenumbers, one has to change W_0 into $-W_0$. In this table are also given the frequency, the wavenumber and the coupling coefficient ζ of the principal modes. Again, one can check that ζ is very close to $\frac{9}{16} \sim 0.5625$ for all these modes and the closest for the largest k .

As seen on the growth rate formula (3), viscosity is always stabilizing. Moreover, viscous damping increases as k increases: the most unstable principal modes are therefore expected to have a small axial wavenumber. The marginal curves for a few couples of azimuthal wavenumbers (m_1, m_2) are plotted in Fig. 3. The principal mode $(0, 2, 1)$ is seen to be always the first mode to be destabilized for $W_0 > 0$. Surpris-

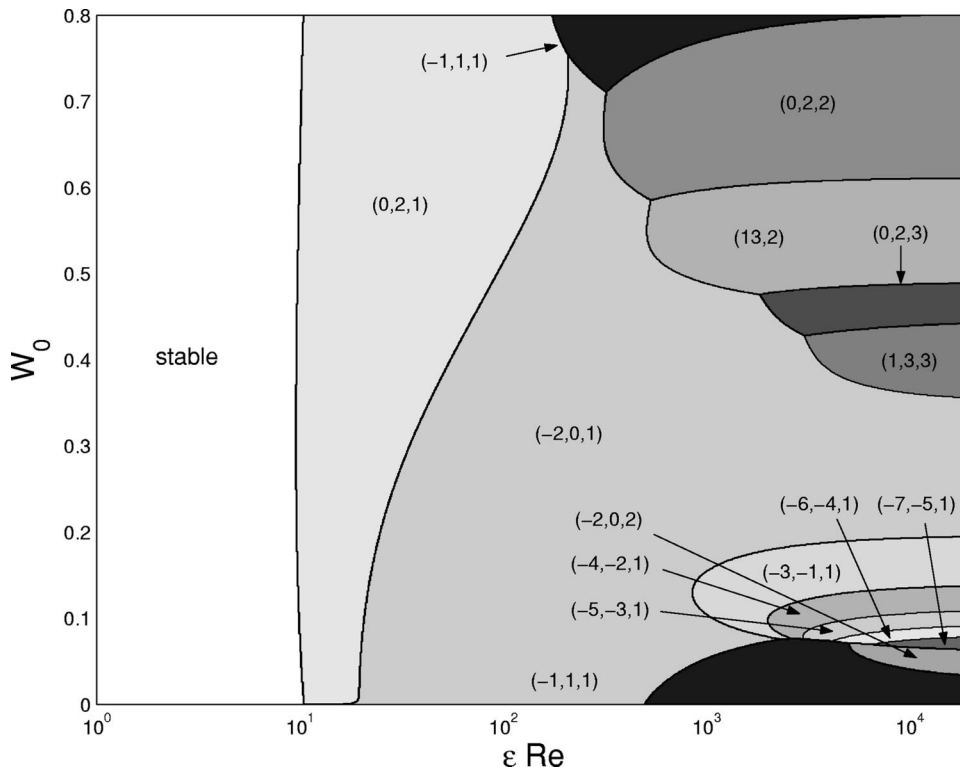


FIG. 6. Most unstable mode in the (W_0, Re) plane.

ingly, this occurs for a value of εRe which is almost independent of W_0 (for $0 < W_0 < 0.8$) and close to 10.

Note that the classical principal mode $(-1, 1, 1)$ is destabilized for much larger values of εRe . Note also that as εRe increases, more and more principal modes are destabilized. But the first mode to be destabilized does not always remain the most unstable mode.

In Fig. 4, the normalized viscous growth rate σ/ε is plotted for the most unstable modes when $\varepsilon \text{Re}=950$. In this figure, one can see that four different principal modes become the most unstable as W_0 varies. The bold line represents the maximum growth rate versus W_0 for $\varepsilon \text{Re}=950$. It is worth noticing that for this value of εRe there exist a most dangerous axial parameter $W_{0c} \approx 0.25$ for which the maximum growth rate is the largest.

The variations of W_{0c} and of the corresponding growth rate versus εRe are shown in Fig. 5. The distribution of the most unstable modes in the parameter plane $(\varepsilon \text{Re}, W_0)$ is given in Fig. 6. One can notice that the larger εRe , the more important is the number of most unstable modes. This results from the weakening of the selective character of viscosity. The mode selection for large εRe is indeed associated with variation of the coupling coefficient ζ . In particular, one expects the ideally resonant modes whose characteristics are given in Table II and which exhibit the largest nonviscous growth rate to appear for sufficiently large εRe . This is visible on the right side of Fig. 6.

IV. CONCLUSION

In this paper, we have analyzed the stability of a strained Rankine vortex with axial flow with respect to the elliptic instability for small strain field, following the analysis of Tsai and Widnall.¹¹ The marginal stability curve and the complete diagram of instability providing the most unstable mode have been obtained as functions of viscosity and axial flow.

The effect of axial flow has been shown to be important. By breaking the symmetry of the dispersion relation, it fundamentally modifies the nature of the resonant modes. Con-

trarily to the case without axial flow, the most unstable modes for large εRe , are not always principal modes with azimuthal wavenumbers $m=-1$ and $m=1$. Instead, various unstable modes with higher azimuthal wavenumbers have been shown to exist depending on the value of W_0 . However, all these modes exhibit a same property. Their frequency satisfies the condition (4) of ideal resonance which is deduced from a maximization of the local instability.

- ¹R. R. Kerswell, "Elliptical instability," *Annu. Rev. Fluid Mech.* **34**, 83 (2002).
- ²T. Leweke and C. H. K. Williamson, "Cooperative elliptic instability of a vortex pair," *J. Fluid Mech.* **360**, 85 (1998).
- ³P. Meunier and T. Leweke, "Three-dimensional instability during vortex merging," *Phys. Fluids* **13**, 2747 (2001).
- ⁴D. Sipp and L. Jacquin, "Widnall instabilities in vortex pairs," *Phys. Fluids* **15**, 1861 (2003).
- ⁵S. Le Dizès and F. Laporte, "Theoretical predictions for the elliptic instability in a two-vortex flow," *J. Fluid Mech.* **471**, 169 (2002).
- ⁶D. Fabre and L. Jacquin, "Short-wave cooperative instabilities in representative aircraft vortices," *Phys. Fluids* **16**, 1366 (2004).
- ⁷G. K. Batchelor, "Axial flow in trailing line vortices," *J. Fluid Mech.* **20**, 645 (1964).
- ⁸P. R. Spalart, "Airplane trailing vortices," *Annu. Rev. Fluid Mech.* **30**, 107 (1998).
- ⁹M. Lessen, N. V. Deshpande, and B. Hadji-Ohanes, "Stability of a potential vortex with a non-rotating and rigid-body rotating top-hat jet core," *J. Fluid Mech.* **60**, 459 (1973).
- ¹⁰T. Loiseleux, J. Chomaz, and P. Huerre, "The effect of swirl on jets and wakes: Linear instability of the Rankine vortex with axial flow," *Phys. Fluids* **10**, 1120 (1998).
- ¹¹C.-Y. Tsai and S. E. Widnall, "The stability of short waves on a straight vortex filament in a weak externally imposed strain field," *J. Fluid Mech.* **73**, 721 (1976).
- ¹²D. W. Moore and P. G. Saffman, "The instability of a straight vortex filament in a strain field," *Proc. R. Soc. London, Ser. A* **346**, 413 (1975).
- ¹³C. Eloy and S. Le Dizès, "Stability of the Rankine vortex in a multipolar strain field," *Phys. Fluids* **13**, 660 (2001).
- ¹⁴Y. Fukumoto, "The three-dimensional instability of a strained vortex tube revisited," *J. Fluid Mech.* **493**, 287 (2003).
- ¹⁵F. Gallaire and J.-M. Chomaz, "Instability mechanisms in swirling flows," *Phys. Fluids* **15**, 2622 (2003).
- ¹⁶E. W. Mayer and K. G. Powell, "Viscous and inviscid instabilities of a trailing vortex," *J. Fluid Mech.* **245**, 91 (1992).
- ¹⁷F. Waleffe, "On the three-dimensional instability of strained vortices," *Phys. Fluids A* **2**, 76 (1990).